

On the addition of an $SU(2)$ quadruplet of scalars to the Standard Model

Darius Jurčiukonis^{(1)*} and Luís Lavoura^{(2)†}

⁽¹⁾ Vilnius University, Institute of Theoretical Physics and Astronomy,
Saulėtekio av. 3, Vilnius 10257, Lithuania

⁽²⁾ Universidade de Lisboa, Instituto Superior Técnico, CFTP,
Av. Rovisco Pais 1, 1049-001 Lisboa, Portugal

January 21, 2026

Abstract

We consider the extension of the Standard electroweak Model through an $SU(2)$ quadruplet of scalars with hypercharge either $3/2$ or $1/2$ (with an additional reflection symmetry in the latter case). We establish, through *exact analytical equations*, the boundaries of the phase spaces of the gauge-invariant terms that appear in the (renormalizable) scalar potentials. We devise procedures for the determination of necessary and sufficient bounded-from-below conditions on those potentials; we emphasize that one mostly needs to scan the scalar potential over a few *lines*, instead of *surfaces*, in order to establish the boundedness-from-below; this fact allows one *to reduce by three orders of magnitude the computational time* devoted to that establishment.

1 Introduction

The Standard Model (SM) of the electroweak interactions has gauge symmetry $SU(2) \times U(1)$. It has only one $SU(2)$ doublet of scalar fields. It produces, upon spontaneous gauge-symmetry breaking and the Higgs mechanism, one physical scalar boson. That boson has been discovered in 2012 [1, 2], providing a confirmation of the SM; still, the self-interactions of that boson [3] remain untested. Up to now, no other fundamental boson has yet been discovered, despite some hints [4, 5].

There is no reason why there should be only one doublet of scalars in an $SU(2) \times U(1)$ gauge theory. Physicists have entertained thoughts that there may be more $SU(2)$ doublets, and possibly also singlets—preserving the so-called custodial symmetry of the SM, *i.e.* the tree-level relation $m_W = m_Z \cos \theta_w$, where m_W and m_Z are the masses of the gauge

*E-mail: darius.jurciukonis@tfai.vu.lt

†E-mail: balio@cftp.tecnico.ulisboa.pt

bosons W^\pm and Z^0 , respectively, and θ_w is the weak mixing (or Weinberg) angle. One may consider larger $SU(2)$ multiplets, like triplets [6–9], quadruplets [10], and more [14–16], even though they would violate the custodial symmetry if they acquired vacuum expectation values (VEVs). Large $SU(2)$ scalar multiplets bring about complicated scalar potentials (SPs) with several $SU(2)$ -invariant terms, and those terms may lead to phase spaces¹ with unexpectedly complex shapes [17, 18]. (The same holds true if the gauge group is chosen to be larger than $SU(2) \times U(1)$ [19, 20].) The exploration of those shapes is relevant since SPs must be bounded from below (BFB), lest the theory has no vacuum state. In order to establish that an SP is BFB one must carefully scrutinize all its phase space, and just that phase space.

In this paper we deal on the addition of one $SU(2)$ quadruplet of scalars to the SM. In order to bring about interesting possibilities for its interaction with the doublet of the SM, we consider two possibilities for their relative hypercharges²: either they are equal or the hypercharge of the quadruplet is three times the one of the doublet. The purpose of this paper is to show that, even in these very simple extensions of the scalar sector of the SM, phase spaces with complicated shapes arise; fortunately, however, those shapes may be described by *exact analytical equations*. The establishment of this fact and of those equations constitute the groundbreaking achievement of this work.

It should be mentioned that scalar quadruplets like the ones that we envisage in this paper, *viz.* with hypercharge either $1/2$ or $3/2$, may be useful—when accompanied by large fermionic $SU(2)$ multiplets—to construct effective extensions of the usual seesaw mechanisms for the neutrino masses [15]. Extensions of the scalar sector of the SM will also bring about deviations of the self-interactions of the SM’s scalar boson from their SM values, and it is relevant to check how large such deviations may be [10]. Scalars in large $SU(2)$ representations are also useful to render the coupling of the Higgs boson to a pair of gauge bosons larger than what it is in the SM, if the new scalars are allowed to have VEVs [11].³ Those VEVs do not necessarily alter the ρ parameter [13].

The plan of this paper is as follows. In Section 2 we expound relevant material from Ref. [14]. In Section 3 we determine the phase space for a quadruplet with hypercharge $3/2$. In Section 4 we determine the phase space for a quadruplet with hypercharge $1/2$ and a reflection symmetry. In Section 5 we write down the main conclusions of this work and we offer two suggestions for further research.

This paper has many appendices that, however, do not need to be read in order to understand the relevant computations. In Appendix A we display the expressions of quantities defined in Sections 3 and 4. In Appendix B we discuss the method to discover whether a surface is convex, concave, or has undefined concavity properties. In Appendix C we deal on a further case, which however is of no practical interest because it is unstable under renormalization. In Appendix D (which is not referred to in the main text of the paper) we display the unitarity constraints on the various models.

¹Some physicists call them instead ‘orbit spaces’.

²In a recent paper of ours [21] the hypercharge of the quadruplet was left arbitrary, preventing additional interactions with the doublet.

³See also Ref. [12].

2 Notation

Multiplets: Let

$$\Phi = \begin{pmatrix} a \\ b \end{pmatrix}, \quad (1a)$$

$$\Xi = \begin{pmatrix} c \\ d \\ e \\ f \end{pmatrix} \quad (1b)$$

be a doublet and a quadruplet, respectively, of the gauge group $SU(2)$. In Eqs. (1), a, \dots, f are complex scalar fields. Let T_3 be the third component of isospin, then c has $T_3 = 3/2$, both a and d have $T_3 = 1/2$, both b and e have $T_3 = -1/2$, and f has $T_3 = -3/2$. Let T_- be the lowering operator of isospin, then $T_-a = b/\sqrt{2}$, $T_-c = \sqrt{3/2}d$, $T_-d = \sqrt{2}e$, $T_-e = \sqrt{3/2}f$, and $T_-b = T_-f = 0$.

Invariants: We define $A = |a|^2$, $B = |b|^2$, $C = |c|^2$, $D = |d|^2$, $E = |e|^2$, and $F = |f|^2$. Then, the following quantities are $SU(2)$ -invariant:

$$F_1 = A + B, \quad (2a)$$

$$F_2 = C + D + E + F, \quad (2b)$$

$$F_4 = \frac{A - B}{4} (3C + D - E - 3F) + \left[\frac{ab^*}{2} \left(\sqrt{3} c^*d + 2d^*e + \sqrt{3} e^*f \right) + \text{H.c.} \right], \quad (2c)$$

$$F_5 = \frac{2}{5} \left| \sqrt{3} ce - d^2 \right|^2 + \frac{2}{5} \left| \sqrt{3} df - e^2 \right|^2 + \frac{1}{5} |3cf - de|^2. \quad (2d)$$

The quantities F_1 , F_2 , and F_5 are non-negative, while F_4 may be either positive or negative. All the quantities in Eqs. (2) are invariant under separate rephasings of Φ and Ξ , *i.e.* they are $U(1)$ -invariant irrespective of the hypercharges of the two multiplets.

Dimensionless parameters: We define

$$r = \frac{F_1}{F_2}, \quad (3a)$$

$$\delta = \frac{4F_4}{3F_1 F_2}, \quad (3b)$$

$$\gamma_5 = \frac{F_5}{F_2^2}. \quad (3c)$$

The ranges of these dimensionless parameters are $r \in [0, +\infty[$, $\delta \in [-1, 1]$, and $\gamma_5 \in [0, 9/20]$. Indeed, defining

$$Q_1 = 9 - 9\delta^2 - 20\gamma_5, \quad (4)$$

it is easy to show that Q_1 is non-negative [7].

Gauge $a = 0$: There is an $SU(2)$ gauge where the field a vanishes in all of space–time. In that gauge,⁴

$$F_1 = B, \quad (5a)$$

$$\delta = \frac{3F + E - D - 3C}{3(F + E + D + C)}. \quad (5b)$$

Potential: The renormalizable and $SU(2) \times U(1)$ -invariant scalar potential V of Φ and Ξ is $V = V_2 + V_4$, where $V_2 = \mu_1^2 F_1 + \mu_2^2 F_2$ is bilinear in the scalar fields and

$$V_4 = \frac{\lambda_1}{2} F_1^2 + \frac{\lambda_2}{2} F_2^2 + \lambda_3 F_1 F_2 + \lambda_4 F_4 + \lambda_5 F_5 + V_{4,\text{extra}} \quad (6)$$

is quadrilinear in the scalar fields. In Eq. (6), $\lambda_1, \lambda_2, \dots, \lambda_5$ are real dimensionless coefficients; furthermore, $V_{4,\text{extra}}$ is a piece of V_4 that depends on the specific hypercharge of Ξ ; if that hypercharge is neither 0, nor 3/2, nor 1/2 then $V_{4,\text{extra}}$ vanishes.^{5,6}

3 Quadruplet with hypercharge 3/2

Extra term: Multiplying Φ by itself twice and taking the fully symmetric part of the product, one sees that

$$(\Phi \otimes \Phi \otimes \Phi)_{\text{fully symmetric}} \propto \begin{pmatrix} a^3 \\ \sqrt{3} a^2 b \\ \sqrt{3} a b^2 \\ b^3 \end{pmatrix} \quad (7)$$

is a quadruplet of $SU(2)$. Therefore, if the hypercharge of Ξ is three times the one of Φ , *i.e.* if Ξ has hypercharge 3/2, then

$$V_{4,\text{extra}} = \frac{\xi}{2} I_{3/2} + \text{H.c.}, \quad (8)$$

where ξ is a complex dimensionless coefficient and

$$I_{3/2} = a^3 c^* + \sqrt{3} a^2 b d^* + \sqrt{3} a b^2 e^* + b^3 f^* \quad (9)$$

is $SU(2) \times U(1)$ -invariant. We define the dimensionless non-negative real parameter ϵ as

$$\epsilon = \frac{|I_{3/2}|}{\sqrt{F_1^3 F_2}}. \quad (10)$$

⁴Another interesting gauge is the one where $a = b$ in all of space–time. We have re-done all our computations using that gauge and we have found exactly the same results as in the gauge $a = 0$; in particular, we have obtained in both gauges the same expressions for the quantities in Appendix A; but, computation times for gauge $a = b$ are significantly larger than for gauge $a = 0$.

⁵We assume a normalization of the hypercharge where Φ has hypercharge 1/2.

⁶The case $V_{4,\text{extra}} = 0$ was studied in Ref. [21].

Then,

$$V_{4,\text{extra}} = |\xi| \epsilon \sqrt{F_1^3 F_2} \cos(\arg \xi + \arg I_{3/2}), \quad (11)$$

so that

$$V_4 = F_2^2 \left[\frac{\lambda_1}{2} r^2 + |\xi| \epsilon \cos(\arg \xi + \arg I_{3/2}) r^{3/2} + \left(\lambda_3 + \frac{3}{4} \lambda_4 \delta \right) r + \frac{\lambda_2 + 2\lambda_5 \gamma_5}{2} \right]. \quad (12)$$

Bounds on ϵ^2 : In the gauge where $a = 0$ throughout space-time, $I_{3/2} = b^3 f^*$ and therefore $\epsilon^2 F_1^3 F_2 = B^3 F = F_1^3 F$. Hence,

$$\epsilon^2 = \frac{F}{F + E + D + C}. \quad (13)$$

Utilizing Eq. (13) together with Eq. (5b) for δ in the same gauge, one finds that

$$2\epsilon^2 - 3\delta + 1 = \frac{4C + 2D}{F + E + D + C}, \quad (14a)$$

$$1 + \delta - 2\epsilon^2 = \frac{2D + E}{3(F + E + D + C)} \quad (14b)$$

are both non-negative. Therefore,

$$3\delta - 1 \leq 2\epsilon^2 \leq 1 + \delta. \quad (15)$$

Thus, the maximum possible value of ϵ is 1 and it occurs only when $\delta = 1$. Moreover, $\delta = -1 \Rightarrow \epsilon = 0$.

Parameters x , y , and z : In order to find the phase-space boundary, it is expedient to assume the fields c , d , e , and f to be real⁷ and define

$$x = \frac{c}{\sqrt{c^2 + d^2 + e^2 + f^2}}, \quad (16a)$$

$$y = \frac{d}{\sqrt{c^2 + d^2 + e^2 + f^2}}, \quad (16b)$$

$$z = \frac{e}{\sqrt{c^2 + d^2 + e^2 + f^2}}. \quad (16c)$$

Then,

$$x^2 + y^2 + z^2 = \frac{c^2 + d^2 + e^2}{c^2 + d^2 + e^2 + f^2} \leq 1 \quad (17)$$

and⁸

$$\frac{f}{\sqrt{c^2 + d^2 + e^2 + f^2}} = \sqrt{1 - x^2 - y^2 - z^2}. \quad (18)$$

⁷In all the cases studied in this paper, we have worked numerically with complex fields and found that the phase-space boundaries are the same for complex and real fields.

⁸Without loss of generality one may assume f to be non-negative.

Moreover,

$$\delta = 1 - 2x^2 - \frac{4}{3}y^2 - \frac{2}{3}z^2, \quad (19a)$$

$$\begin{aligned} \gamma_5 = & \frac{1}{5} \left(3x\sqrt{1-x^2-y^2-z^2} - yz \right)^2 \\ & + \frac{2}{5} \left\{ \left(\sqrt{3}xz - y^2 \right)^2 + \left[y\sqrt{3(1-x^2-y^2-z^2)} - z^2 \right]^2 \right\}, \end{aligned} \quad (19b)$$

and

$$\epsilon = \sqrt{1-x^2-y^2-z^2}. \quad (20)$$

Boundary: Referring to Eqs. (19) and (20), if

$$\det \begin{pmatrix} \frac{\partial \delta}{\partial x} & \frac{\partial \delta}{\partial y} & \frac{\partial \delta}{\partial z} \\ \frac{\partial \gamma_5}{\partial x} & \frac{\partial \gamma_5}{\partial y} & \frac{\partial \gamma_5}{\partial z} \\ \frac{\partial \epsilon}{\partial x} & \frac{\partial \epsilon}{\partial y} & \frac{\partial \epsilon}{\partial z} \end{pmatrix} = 0, \quad (21)$$

then one is at the boundary of the $(\delta, \gamma_5, \epsilon)$ phase space. Equation (21) states that the gradients of δ , γ_5 , and ϵ are linearly dependent and thus span a surface—the border of phase space—instead of a volume, as they do when the determinant in the left-hand side of Eq. (21) is nonzero. Equation (21) is an equation among x , y , and z that one may convert into an equation among δ , γ_5 , and ϵ by inverting Eqs. (19) and (20). In this way we have obtained the equation⁹

$$Q_1 \epsilon^2 Q_2 = 0, \quad (22)$$

where Q_1 is the quantity defined in Eq. (4) and Q_2 is a polynomial function of δ , γ_5 , and ϵ^2 explicitly given in Appendix A. In practice, the border of the allowed volume is formed by three sheets:

1. Sheet 1 has equation $Q_1 = 0$.
2. Sheet 2 has equation $\epsilon = 0$.
3. Sheet 3 has equation $Q_2 = 0$.

⁹Writing Eq. (21) in terms of δ , γ_5 , and ϵ is a non-trivial task that we were able to accomplish by having recourse to the Gröbner basis.

Points: We define the points

$$\tilde{P}_1 : \quad \delta = -1, \quad \gamma_5 = \epsilon = 0; \quad (23a)$$

$$\tilde{P}_2 : \quad \delta = \frac{1}{3}, \quad \gamma_5 = \frac{2}{5}, \quad \epsilon = 0; \quad (23b)$$

$$\tilde{P}_3 : \quad \delta = \epsilon = 1, \quad \gamma_5 = 0; \quad (23c)$$

$$\tilde{P}_4 : \quad \delta = \frac{3 + 4\sqrt{3}}{13}, \quad \gamma_5 = \frac{18(14 - 3\sqrt{3})}{845}, \quad \epsilon^2 = \frac{11 + 6\sqrt{3}}{26}; \quad (23d)$$

$$\tilde{P}_5 : \quad \delta = 0, \quad \gamma_5 = \frac{9}{20}, \quad \epsilon^2 = \frac{1}{2}. \quad (23e)$$

All these points are located on the boundary of phase space. Both \tilde{P}_1 and \tilde{P}_2 have $Q_1 = Q_2 = \epsilon = 0$; the other three points have $Q_1 = Q_2 = 0$ but $\epsilon \neq 0$.

Lines: We define three lines linking \tilde{P}_1 to \tilde{P}_2 through different paths:

- The blue line has equation $Q_1 = \epsilon = 0$.
- The purple line is given by $Q_2 = \epsilon = 0$. According to the expression for Q_2 given in Appendix A, this means that for the purple line

$$256(10\gamma_5)^3 - 32(89 + 90\delta + 81\delta^2)(10\gamma_5)^2 \quad (24a)$$

$$+ 9(1129 + 2868\delta + 4614\delta^2 + 3348\delta^3 + 729\delta^4)(10\gamma_5) \quad (24b)$$

$$- 81(1 + \delta)^3(127 + 225\delta + 405\delta^2 + 243\delta^3) = 0. \quad (24c)$$

Equation (24) implicitly gives, together with $\epsilon = 0$, the purple line.

- The magenta–green–brown line is given by $Q_1 = Q_2 = 0$. It has three segments:
 - The magenta segment begins at \tilde{P}_1 and ends at \tilde{P}_3 . It has

$$\epsilon^2 = \frac{1 + \delta}{2}. \quad (25)$$

The point \tilde{P}_5 lies between \tilde{P}_1 and \tilde{P}_3 on the magenta segment.

- The green segment begins at \tilde{P}_3 and ends at \tilde{P}_4 . It has

$$\epsilon^2 = \frac{1 + 3\delta}{4}. \quad (26)$$

- The brown segment begins at \tilde{P}_4 and ends at \tilde{P}_2 . It has

$$\epsilon^2 = \frac{(3\delta - 1)(7\delta + 3)^3}{2048\delta^3}. \quad (27)$$

All three segments have $Q_1 = 0$, *viz.* $\gamma_5 = 9(1 - \delta^2)/20$. We note that at their meeting point \tilde{P}_4 the green and brown segments have continuous first derivative

$$\frac{d\epsilon}{d\delta}\bigg|_{\tilde{P}_4} = \frac{3\sqrt{2}}{8} \sqrt{11 - 6\sqrt{3}}, \quad (28)$$

but different second derivatives:

$$\frac{d^2\epsilon_{\text{green}}}{(d\delta)^2}\bigg|_{\tilde{P}_4} = -\frac{117\sqrt{26}}{32(\sqrt{11 + 6\sqrt{3}})^3}, \quad (29a)$$

$$\frac{d^2\epsilon_{\text{brown}}}{(d\delta)^2}\bigg|_{\tilde{P}_4} = \frac{2(9 + 7\sqrt{3})}{9} \frac{d^2\epsilon_{\text{green}}}{(d\delta)^2}\bigg|_{\tilde{P}_4}. \quad (29b)$$

On the other hand, at the point \tilde{P}_3 the magenta–green–brown line changes $d\epsilon/d\delta$. Referring to the inequalities (15) we note that the upper bound $2\epsilon^2 \leq 1 + \delta$ is saturated at the magenta segment of this line.

Bounding surface: The surface bounding phase space has the topology of the surface of a sphere. The “poles” are \tilde{P}_1 and \tilde{P}_2 . The surface is formed by sheet 1, followed by the blue line, followed by sheet 2, followed by the purple line, followed by the sheet 3, followed by the magenta–green–brown line, then returning to sheet 1.

Auxiliary lines: It is useful to define two other lines, which have $Q_2 = 0$ but neither $Q_1 = 0$ nor $\epsilon = 0$, *i.e.* they lie on sheet 3.

- The orange line is defined by

$$\gamma_5 = \frac{9(\delta - 1)^2}{10}, \quad (30a)$$

$$\epsilon^2 = \frac{3\delta - 1}{2}. \quad (30b)$$

The orange line starts at \tilde{P}_2 and ends at \tilde{P}_3 . The lower bound $2\epsilon^2 \geq 3\delta - 1$ is saturated at the orange line for $1/3 \leq \delta \leq 1$; for $-1 \leq \delta \leq 1/3$ the lower bound on ϵ^2 is simply $\epsilon^2 \geq 0$ and is saturated at sheet 2.

- The yellow line is defined by

$$\gamma_5 = 0, \quad (31a)$$

$$\epsilon^2 = \frac{(1 + \delta)^3}{8}. \quad (31b)$$

The yellow line starts at \tilde{P}_1 and ends at \tilde{P}_3 . It saturates the bound $\gamma_5 \geq 0$.

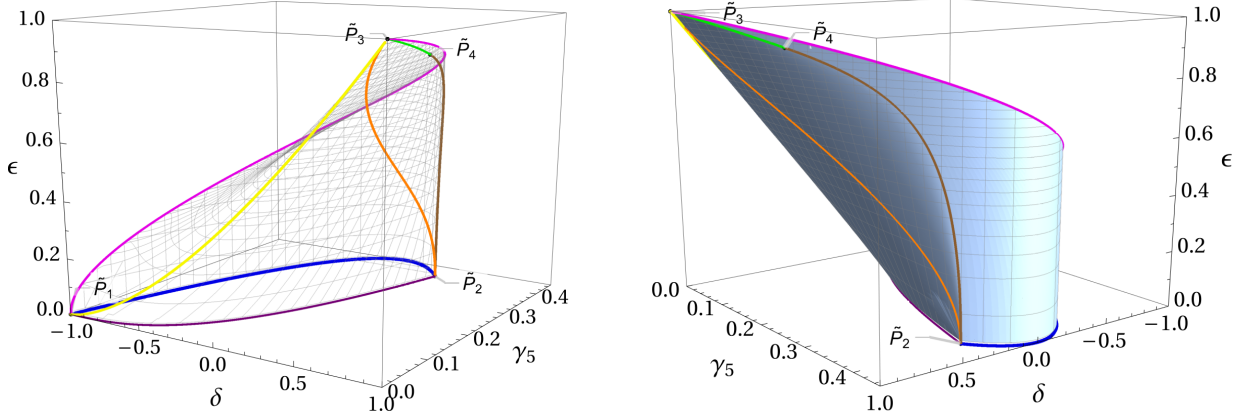


Figure 1: Two perspectives of the phase space for case $Y = 3/2$. The lines and the points—except \tilde{P}_5 —defined in the text are explicitly displayed. In the left panel the phase space is displayed transparent, so that the lines may be seen behind each other; in the right panel it is opaque.

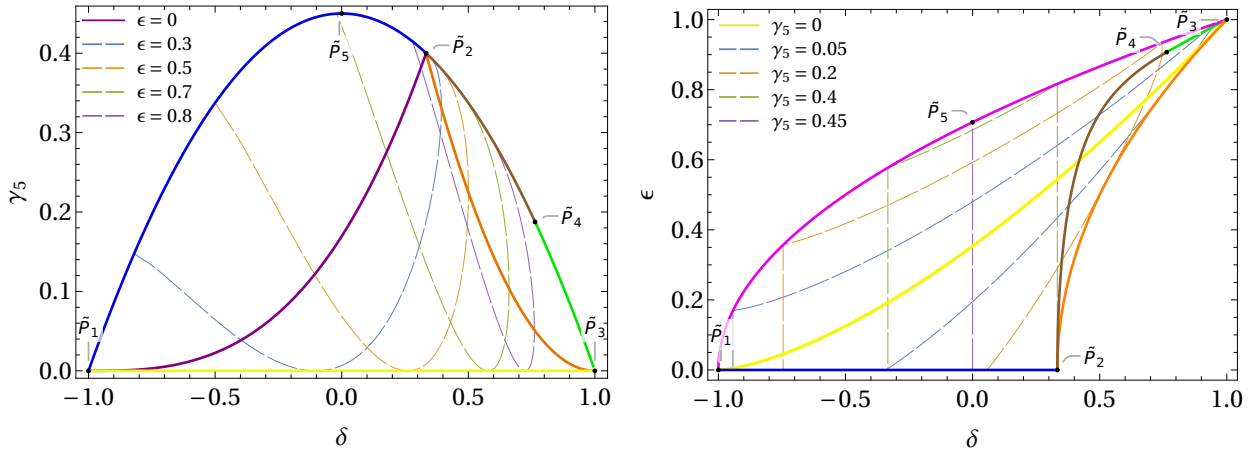


Figure 2: The projections of the phase space for case $Y = 3/2$ on the planes γ_5 vs. δ (left panel) and ϵ vs. δ (right panel). See further comments on this figure in the text.

Figures: Figure 1 has two panels with different perspectives of phase space. Figure 2 shows two projections of the phase space on planes. On the left panel of that figure, note the following.

1. The magenta segment coincides with the union of the blue line, the brown segment, and the green segment.
2. Sheet 1 is wholly projected on the blue line and on the brown and green segments. Sheet 2 is the left part of the surface, between the blue and purple lines. Sheet 3 is the whole space under the parabola.

3. The dashed lines (and the full purple line for $\epsilon = 0$) display the contours of constant ϵ *on sheet 3*.

On the right panel of Fig. 2 note the following.

1. The purple line coincides with the blue line.
2. Sheet 2 is wholly projected onto the blue line. Sheet 3 occupies the whole triangle among the blue and orange lines and the magenta segment. Sheet 1 only occupies the left part of the triangle, between the blue line and the magenta–green–brown line.
3. Besides the full yellow line with $\gamma_5 = 0$, there are dashed lines of constant γ_5 ; they are vertical on sheet 1 and curved on sheet 3, explicitly displaying the concavity of that sheet.

Boundedness from below: The potential is BFB if and only if $V_4 \geq 0$ for any values of the fields.¹⁰ Referring to Eq. (12) and taking into account that the fields may take phases such that $\cos(\arg \xi + \arg I_{3/2}) = -1$, we require that

$$\frac{V_4}{F_2^2} = c_4 (\sqrt{r})^4 + c_3 (\sqrt{r})^3 + c_2 (\sqrt{r})^2 + c_0 \geq 0 \quad (32)$$

for every $\sqrt{r} > 0$, where

$$c_4 = \frac{\lambda_1}{2}, \quad c_3 = -|\xi| \epsilon, \quad c_2 = \lambda_3 + \frac{3}{4} \lambda_4 \delta, \quad c_0 = \frac{\lambda_2 + 2\lambda_5 \gamma_5}{2}. \quad (33)$$

Note the crucial facts that there is no term $c_1 \sqrt{r}$ in Eq. (32) and that $c_3 \leq 0$ in Eq. (33). By considering the cases $\sqrt{r} \rightarrow \infty$ and $\sqrt{r} \rightarrow 0$, condition (32) of course requires $c_4 \geq 0$ and $c_0 \geq 0$, respectively, *i.e.*

$$\lambda_1 \geq 0, \quad (34a)$$

$$\lambda_2 + 2\lambda_5 \gamma_5 \geq 0. \quad (34b)$$

Since the left-hand side of condition (34b) is a monotonic function of γ_5 , that condition holds for all γ_5 if and only if it holds for the maximal and minimal γ_5 , *i.e.* if conditions

$$\lambda_2 \geq 0, \quad (35a)$$

$$\lambda_2 + \frac{9}{10} \lambda_5 \geq 0 \quad (35b)$$

hold true. We next apply Theorem 2 of Ref. [23], which states¹¹ that condition (32) holds $\forall \sqrt{r} > 0$ if and only if

¹⁰A stricter definition of boundedness-from-below requires V_4 to be strictly positive. In this paper we are a bit sloppy; we do not pay much attention to the possibilities of strict equality, which are anyway meaningless under renormalization.

¹¹The theorem also applies to the case $c_1 \neq 0$, so we are using here a simplified version thereof.

1. either

$$\Delta \leq 0 \text{ and } \aleph > 0, \quad (36)$$

2. or

$$\Delta \geq 0 \text{ and } \begin{cases} \text{either } -2 \leq \beth \leq 6 \text{ and } \Lambda_1 \leq 0, \\ \text{or } \beth > 6 \text{ and } \Lambda_2 \leq 0. \end{cases} \quad (37)$$

Here,

$$\Delta = 4(\beth^2 + 12)^3 - (2\beth^3 - 72\beth + 27\aleph^2)^2, \quad (38a)$$

$$\Lambda_1 = \aleph^2 - 16\aleph - 16(\beth + 2), \quad (38b)$$

$$\Lambda_2 = \aleph^2 - 4\aleph \frac{\beth + 2}{\sqrt{\beth - 2}} - 16(\beth + 2), \quad (38c)$$

where

$$\aleph = \frac{c_3}{\sqrt[4]{c_4^3 c_0}}, \quad (39a)$$

$$\beth = \frac{c_2}{\sqrt{c_4 c_0}}. \quad (39b)$$

Since $c_3 \leq 0$, $\aleph \leq 0$ and possibility (36) may be discarded, so only option (37) remains. That option necessitates $\beth \geq -2$, which is precisely the condition $c_2 \geq -2\sqrt{c_4 c_0}$ that also applies when $c_3 = 0$. Hence, the following necessary BFB conditions [21] apply:

$$\lambda_3 - \frac{3|\lambda_4|}{4} + \sqrt{\lambda_1 \lambda_2} \geq 0, \quad (40a)$$

$$\lambda_3 + \sqrt{\lambda_1 \left(\lambda_2 + \frac{9}{10} \lambda_5 \right)} \geq 0. \quad (40b)$$

Furthermore, one must *impede* the situation where

$$8\lambda_1 \lambda_5 < -5\lambda_4^2, \quad (41a)$$

$$6\sqrt{\lambda_1} \lambda_5 < -5\sqrt{\lambda_2} |\lambda_4|, \quad (41b)$$

$$\lambda_3 < -\sqrt{\frac{(10\lambda_2 + 9\lambda_5)(8\lambda_1 \lambda_5 + 5\lambda_4^2)}{80\lambda_5}} \quad (41c)$$

simultaneously. We next consider the constraints on \aleph in condition (37). Since $\Delta \geq 0$,

$$\frac{2}{27} \left[\beth (36 - \beth^2) - (\sqrt{\beth^2 + 12})^3 \right] \leq \aleph^2 \leq \frac{2}{27} \left[\beth (36 - \beth^2) + (\sqrt{\beth^2 + 12})^3 \right]. \quad (42)$$

Furthermore, either

$$-2 \leq \beth \leq 6 \quad \text{and} \quad 0 \geq \aleph \geq -4 \left(\sqrt{\beth + 6} - 2 \right) \quad (43)$$

or

$$\square > 6 \quad \text{and} \quad 0 \geq \aleph \geq -2 \sqrt{\frac{\square + 2}{\square - 2}} \left(\sqrt{5\square - 6} - \sqrt{\square + 2} \right). \quad (44)$$

Since inequalities (43) and (44) effectively impose lower bounds on \aleph , they must apply to

$$\aleph = \frac{-2 |\xi| \epsilon_{\max}(\delta, \gamma_5)}{\sqrt[4]{\lambda_1^3 (\lambda_2 + 2\lambda_5 \gamma_5)}}, \quad (45)$$

where $\epsilon_{\max}(\delta, \gamma_5)$ is the maximum possible value of ϵ for each δ and γ_5 ; clearly, this is always given by a solution of equation $Q_2 = 0$, hence the exact expression for Q_2 in Appendix A is relevant.

Importance of the magenta line: By following the procedure described in Appendix B we have found that sheet 3 has both a (rather small) concave part and a (much larger) part which is neither concave nor convex; sheet 3 has no convex part. As a consequence, one needs to check conditions (42)–(44) *only along the boundaries of the surface*, specifically along the magenta and yellow lines. As a matter of fact, our numerical computations—performed with 10^6 randomly generated sets of parameters $\lambda_1, \dots, \lambda_5, |\xi|$ —indicate that the scan along the yellow line is superfluous: it is sufficient to scan *the magenta line*, *i.e.* it is sufficient to use

$$\aleph = \frac{-|\xi| \sqrt{2(1+\delta)}}{\sqrt[4]{\lambda_1^3 [\lambda_2 + 9(1-\delta^2) \lambda_5/10]}}, \quad (46a)$$

$$\square = \frac{4\lambda_3 + 3\lambda_4 \delta}{2\sqrt{\lambda_1 [\lambda_2 + 9(1-\delta^2) \lambda_5/10]}} \quad (46b)$$

with $-1 \leq \delta \leq 1$. Thus, our practical recipe for ascertaining the boundedness-from-below of V_4 consists of the following successive steps:

1. Checking the necessary conditions (34a), (35), and (40).
2. Discarding any case where conditions (41) apply.
3. Testing conditions (42)–(44) at the special points (23).
4. Testing conditions (42)–(44) with \aleph and \square given by Eqs. (46) for $\delta \in [-1, 1]$.

Step 4 must, of course, be performed numerically and with sufficiently small steps of δ .

Efficiency of the method: In order to demonstrate the efficiency of our method, we have compared it with the direct minimization of V_4 . We have randomly generated 10^6 sets of couplings $\lambda_3, \lambda_4, \lambda_5, \xi \in [-10, 10]$ and $\lambda_1, \lambda_2 \in [0, 10]$, being careful to ensure that the distribution of each coupling over its respective range is uniform. The potential V_4 was then minimized¹² for each set of couplings. Alternatively, we have used our recipe given in the previous paragraph. Our results were:

¹²In order to ensure high accuracy, we have employed two minimization algorithms—specifically, the Nelder–Mead method and the Differential Evolution method. The minimization was made over *real* fields a, b, \dots, f , letting those fields vary over various ranges—for instance, from -1 to 1 , from -100 to 100 , and from -10^5 to 10^5 ; by doing this we aimed at not missing any minimum, independently of it having small or large values of the fields.

- The minimization of V_4 for the 10^6 sets of parameters required 39 516 seconds,¹³ producing 256 179 quartic potentials that are bounded from below.
- Our scanning method completed the task in 29.2 seconds, yielding exactly the same 256 179 BFB potentials.

This comparison demonstrates that our method is approximately 1 300 times faster than the brute-force minimization of the potential and suggests that it is just as exact.

4 Quadruplet with hypercharge 1/2 and a reflection symmetry

Extra term: Multiplying the doublet Φ by itself one obtains the $SU(2)$ triplet

$$T_1 = (\Phi \otimes \Phi)_{\mathbf{3}} = \begin{pmatrix} a^2 \\ \sqrt{2}ab \\ b^2 \end{pmatrix}. \quad (47)$$

Multiplying the quadruplet Ξ by itself one also obtains (besides a seven-plet) an $SU(2)$ triplet:

$$T_2 = (\Xi \otimes \Xi)_{\mathbf{3}} = \frac{1}{\sqrt{5}} \begin{pmatrix} \sqrt{6}ce - \sqrt{2}d^2 \\ 3cf - de \\ \sqrt{6}df - \sqrt{2}e^2 \end{pmatrix}. \quad (48)$$

If the hypercharge of Ξ is the same as the one of Φ , *i.e.* if Ξ has hypercharge 1/2, then one may construct an $SU(2) \times U(1)$ -invariant quantity out of the triplets (47) and (48):

$$I_{1/2} = \sqrt{\frac{2}{5}} \left[a^{*2} \left(\sqrt{3}ce - d^2 \right) + a^*b^* (3cf - de) + b^{*2} \left(\sqrt{3}df - e^2 \right) \right]. \quad (49)$$

If moreover the Lagrangian is symmetric under $\Xi \rightarrow -\Xi$,¹⁴ then

$$V_{4,\text{extra}} = \frac{\chi}{2} I_{1/2} + \text{H.c.}, \quad (51)$$

¹³Our computations were performed on a desktop computer equipped with an Intel Core i9-13900K CPU featuring 24 cores. All the cases being compared were evaluated under identical conditions by using **Mathematica**, with calculations executed in parallel across all cores.

¹⁴The extra symmetry is needed to remove the terms

$$\left[(\Xi \otimes \Xi)_{\mathbf{3}} \otimes \left(\tilde{\Xi} \otimes \tilde{\Phi} \right)_{\mathbf{3}} \right]_1, \quad (50a)$$

$$\left[(\Phi \otimes \Phi)_{\mathbf{3}} \otimes \left(\tilde{\Xi} \otimes \tilde{\Phi} \right)_{\mathbf{3}} \right]_1, \quad (50b)$$

that in general are also present in the SP if Ξ and Φ have the same hypercharge. In the expressions (50), $\tilde{\Phi}$ and $\tilde{\Xi}$ are the $SU(2)$ doublet and the $SU(2)$ quadruplet, respectively, formed by the complex conjugates of the fields a, \dots, f .

where χ is a complex dimensionless coefficient. We define the dimensionless non-negative real parameter η as

$$\eta = \frac{|I_{1/2}|}{F_1 F_2}. \quad (52)$$

Then,

$$V_{4,\text{extra}} = |\chi| \eta F_1 F_2 \cos(\arg \chi + \arg I_{1/2}), \quad (53)$$

so that

$$V_4 = F_2^2 \left\{ \frac{\lambda_1}{2} r^2 + \left[\lambda_3 + \frac{3}{4} \lambda_4 \delta + |\chi| \eta \cos(\arg \chi + \arg I_{1/2}) \right] r + \frac{\lambda_2 + 2\lambda_5 \gamma_5}{2} \right\}. \quad (54)$$

Upper bounds on η : In the gauge where $a = 0$, $I_{1/2} = \sqrt{2/5} b^{*2} (\sqrt{3} df - e^2)$ and therefore $\eta^2 F_1^2 F_2^2 = (2/5) B^2 |\sqrt{3} df - e^2|^2 = (2/5) F_1^2 |\sqrt{3} df - e^2|^2$. Hence,

$$\eta^2 = \frac{2 |\sqrt{3} df - e^2|^2}{5 (F + E + D + C)^2}, \quad (55)$$

which should be used together with Eq. (5b). One then finds that

$$Q_3 = 9(1 + \delta)^2 - 40\eta^2 \quad (56a)$$

$$= \frac{4(3F - D)^2 + 16 |d^* e + \sqrt{3} e^* f|^2}{(F + E + D + C)^2} \quad (56b)$$

$$\geq 0. \quad (56c)$$

Therefore,

$$\eta^2 \leq \frac{9(1 + \delta)^2}{40}. \quad (57)$$

Another upper bound on η is

$$\eta^2 \leq \gamma_5, \quad (58)$$

which directly follows from Eqs. (2b), (2d), (3c), and (55).

Boundary: We assume c, d, e , and f to be real instead of complex and we define the real parameters x, y , and z through Eqs. (16). Then,

$$\eta^2 = \frac{2}{5} \left[y \sqrt{3(1 - x^2 - y^2 - z^2)} - z^2 \right]^2, \quad (59)$$

which should be used together with Eqs. (19). A point where

$$\det \begin{pmatrix} \frac{\partial \delta}{\partial x} & \frac{\partial \delta}{\partial y} & \frac{\partial \delta}{\partial z} \\ \frac{\partial \gamma_5}{\partial x} & \frac{\partial \gamma_5}{\partial y} & \frac{\partial \gamma_5}{\partial z} \\ \frac{\partial \eta^2}{\partial x} & \frac{\partial \eta^2}{\partial y} & \frac{\partial \eta^2}{\partial z} \end{pmatrix} = 0 \quad (60)$$

is a candidate to lie at the boundary of the (δ, γ_5, η) phase space. Equation (60) translates into

$$Q_1 Q_3 Q_4 \eta^2 = 0, \quad (61)$$

where Q_1 was defined in Eq. (4), Q_3 was defined in Eq. (56a), and Q_4 is a polynomial function of δ , γ_5 , and η^2 that is explicitly written down in Appendix A. In practice, the boundary of phase space is formed by four sheets:

1. Sheet 1 has equation $Q_1 = 0$.
2. Sheet 2 has equation $Q_3 = 0$.
3. Sheet 3 has equation $Q_4 = 0$.
4. Sheet 4 has equation $\eta = 0$.

Points: We define the points

$$\bar{P}_1 : \quad \delta = -1, \quad \gamma_5 = \eta = 0; \quad (62a)$$

$$\bar{P}_2 : \quad \delta = \frac{1}{3}, \quad \gamma_5 = \eta^2 = \frac{2}{5}; \quad (62b)$$

$$\bar{P}_3 : \quad \delta = \frac{1+2\sqrt{2}}{7}, \quad \gamma_5 = \frac{9(10-\sqrt{2})}{245}, \quad \eta^2 = \frac{9(9+4\sqrt{2})}{490}; \quad (62c)$$

$$\bar{P}_4 : \quad \delta = \frac{2}{3}, \quad \gamma_5 = \frac{1}{4}, \quad \eta^2 = \frac{9}{40}; \quad (62d)$$

$$\bar{P}_5 : \quad \delta = 1, \quad \gamma_5 = \eta = 0. \quad (62e)$$

All these points are located on the boundary of phase space. Point \bar{P}_1 has $Q_1 = Q_3 = Q_4 = \eta = 0$. Point \bar{P}_2 has $Q_1 = Q_3 = Q_4 = 0$ but $\eta \neq 0$. Point \bar{P}_5 has $Q_1 = Q_4 = \eta = 0$ but $Q_3 \neq 0$. Both point \bar{P}_3 and point \bar{P}_4 have $Q_1 = Q_4 = 0$ but $Q_3 \neq 0$ and $\eta \neq 0$.

Lines: We define two lines linking \bar{P}_1 to \bar{P}_2 through different paths:

- The magenta line is given by $Q_1 = Q_3 = 0$.
- The purple line is given by $Q_3 = Q_4 = 0$, *viz.* by

$$\gamma_5 = \frac{9(3-\delta)(1+\delta)}{80}, \quad (63a)$$

$$\eta = \frac{3(1+\delta)}{2\sqrt{10}}. \quad (63b)$$

We furthermore define two lines linking \bar{P}_1 to \bar{P}_5 through different paths:

- The blue line is given by $Q_1 = \eta = 0$.
- The yellow line is given by $Q_4 = \eta = \gamma_5 = 0$.

Finally, we define the green–brown line, which has $Q_1 = Q_4 = 0$ and connects \overline{P}_2 to \overline{P}_5 . This line has two segments¹⁵:

- The brown segment goes from \overline{P}_2 to \overline{P}_3 . It has $Q_1 = 0$ and

$$\eta = \frac{3(1+\delta)^2}{8\sqrt{10}\delta}. \quad (64)$$

- The green segment goes from \overline{P}_3 to \overline{P}_5 . It has $Q_1 = 0$ and

$$\eta = \frac{3\sqrt{(3\delta+1)(1-\delta)}}{2\sqrt{10}}. \quad (65)$$

The point \overline{P}_4 lies on the green segment.

At the point \overline{P}_3 where they meet, the green and brown segments have equal first derivative

$$\frac{d\eta}{d\delta}\bigg|_{\overline{P}_3} = -\frac{3\sqrt{5}}{10}\sqrt{3-2\sqrt{2}}, \quad (66)$$

but symmetric second derivatives:

$$\frac{d^2\eta_{\text{brown}}}{(d\delta)^2}\bigg|_{\overline{P}_3} = -\frac{d^2\eta_{\text{green}}}{(d\delta)^2}\bigg|_{\overline{P}_3} = \frac{3\sqrt{5}}{40}\sqrt{44-25\sqrt{2}}. \quad (67)$$

Bounding surface: The surface that bounds phase space has the topology of the surface of a sphere. The three points \overline{P}_1 , \overline{P}_2 , and \overline{P}_5 form a triangle on that surface. The sides of the triangle are the purple, yellow, and green–brown lines. The magenta line and the blue line lie inside the triangle. The whole surface outside the triangle has $Q_4 = 0$, *i.e.* it is sheet 3. Inside the triangle there is sheet 2 between the purple and magenta lines, sheet 4 between the yellow and blue lines, and sheet 1 among the magenta, blue, and green–brown lines.

Orange line: The upper bound (57) on η^2 gets saturated at the magenta line for $-1 \leq \delta \leq 1/3$. For $1/3 \leq \delta \leq 1$ the relevant upper bound on η^2 is (58), which is saturated at the orange line. This is defined by

$$\gamma_5 = \eta^2 = \frac{9(1-\delta)^2}{10}. \quad (68)$$

The orange line goes from \overline{P}_2 to \overline{P}_5 just as the green–brown line. It has $Q_4 = 0$ but $Q_1 \neq 0$, $Q_3 \neq 0$, and $\eta \neq 0$, so it is outside the triangle defined in the previous paragraph.

¹⁵The equations for the green segment and for the brown segment are distinct solutions of $Q_1 = Q_4 = 0$. Since Q_4 is a high-order polynomial, it has various roots, out of which two are relevant for sheet 3.

Concavity and the red line: Sheet 2 is flat: it is on the plane $2\sqrt{10}\eta = 3(1+\delta)$. Following the procedure described in Appendix B, we have found that sheet 3 consists both of a convex region and of a region that is neither concave nor convex. These two regions are separated by the red line, defined by

$$\gamma_5 = \frac{5 - \sqrt{7 - 18\delta}}{10}, \quad (69a)$$

$$\eta = \frac{8 + 3\delta - \sqrt{7 - 18\delta}}{4\sqrt{10}} \quad (69b)$$

for $-1 \leq \delta \leq 1/3$. The red line lies on the plane $4\sqrt{10}\eta = 3 + 3\delta + 10\gamma_5$. The portion of sheet 3 between the purple and red lines is neither convex nor concave; the portion of sheet 3 between the red and green–brown lines is convex.

Figures: The surface that bounds phase space is displayed in Fig. 3 from two different perspectives. In Fig. 4 we display the projection of that surface on the γ_5 vs. δ plane; in this

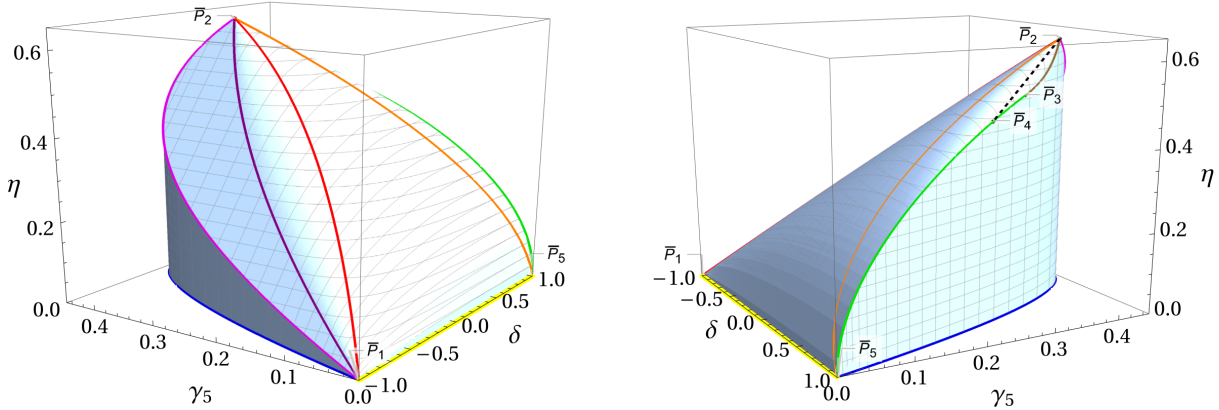


Figure 3: Two perspectives of the boundary of phase space for case $Y = 1/2$ with reflection symmetry. The points and lines defined in the text are explicitly displayed.

projection, the blue line—which is not displayed in Fig. 4—coincides with the magenta line for $\delta < 1/3$ and with the green–brown line for $\delta > 1/3$.

Black dashed line: Equation $Q_4 = 0$ in general produces six solutions for γ_5 , but only two of those solutions are relevant for bounding the phase space. For $0 \leq \eta^2 \leq 9/40$, sheet 3 is formed by solution $\gamma_5^{(1)}(\delta, \eta)$; for $9/40 \leq \eta^2 \leq 2/5$, sheet 3 is formed partly by solution $\gamma_5^{(1)}(\delta, \eta)$ and partly by solution $\gamma_5^{(2)}(\delta, \eta)$; those two solutions are separated by, and coincide, at the black dashed line. That line is given by

$$\gamma_5 = \frac{11 - 9\delta}{20}, \quad (70a)$$

$$\eta = \frac{5 - 3\delta}{2\sqrt{10}}, \quad (70b)$$

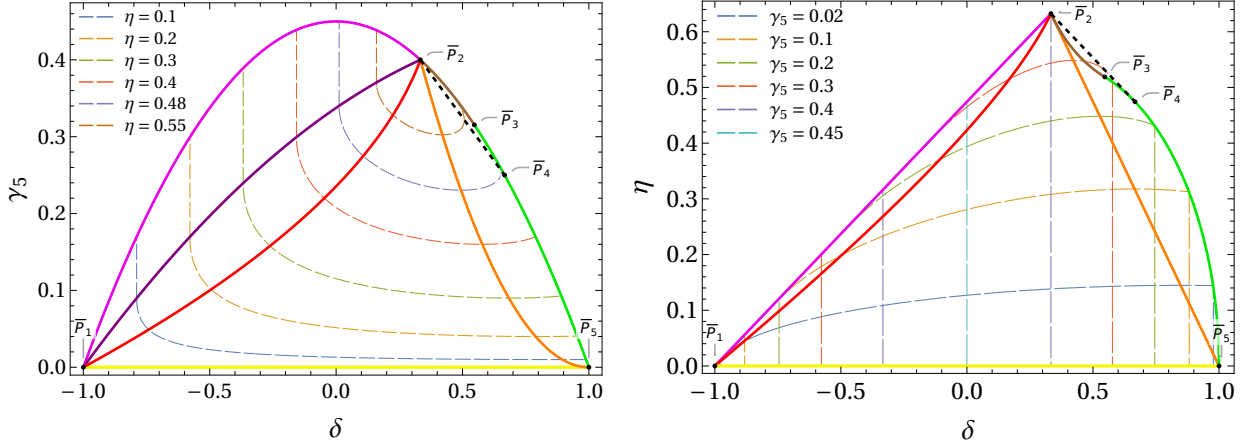


Figure 4: Left panel: the projection of phase space for case $Y = 1/2$ with reflection symmetry onto the γ_5 vs. δ plane. The blue line, which is not displayed, coincides with the magenta and green–brown lines, just as the whole sheet 1 of the boundary of phase space. Sheet 2 is between the magenta and purple lines. Sheet 3 is among the purple, yellow, and green–brown lines. Sheet 4 is the whole area under the parabola. Dashed lines of constant η are marked in various colours. Right panel: the projection of the same phase space onto the η vs. δ plane. The blue line, which is not displayed, coincides with the yellow line, just as the whole sheet 4 of the boundary of phase space. The purple line, which is not displayed, coincides with the magenta line, just as the whole sheet 2 of the boundary of phase space. Sheet 3 is the whole area under the magenta line, black dashed line, and part of the green segment; sheet 1 is the area under the magenta and green–brown lines. Dashed lines of constant γ_5 are marked in various colours.

for $1/3 \leq \delta \leq 2/3$. The black dashed line starts at \bar{P}_2 and ends at \bar{P}_4 , where it meets the green segment of the green–brown line. As seen in Fig. 4, the black dashed line is the locus of the points at the boundary of phase space with maximal δ for a fixed given η , provided that $\eta > 3/(2\sqrt{10})$.

Boundedness from below: The necessary and sufficient conditions for the potential in Eq. (54) to be BFB are conditions (34a), (35) and, besides [22],

$$\lambda_3 + \frac{3}{4} \lambda_4 \delta - |\chi| \eta + \sqrt{\lambda_1 (\lambda_2 + 2\lambda_5 \gamma_5)} \geq 0 \quad (71)$$

must hold for all possible values of δ , γ_5 , and η . Since the term $|\chi| \eta$ appears in condition (71) with negative sign, what matters in practice is the maximum possible η for each value of the pair (δ, γ_5) . So, looking at Fig. 3, what matters are sheets 2 and 3 of the bounding surface. On sheet 2, η is a function only of δ while γ_5 increases monotonously when going from the purple line to the magenta line. One therefore has two further necessary conditions for V_4

to be BFB, namely

$$\lambda_3 + \frac{3}{4} \lambda_4 \delta - |\chi| \frac{3(1+\delta)}{2\sqrt{10}} + \sqrt{\lambda_1 \left[\lambda_2 + \frac{9}{10} \lambda_5 (1-\delta^2) \right]} > 0, \quad (72a)$$

$$\lambda_3 + \frac{3}{4} \lambda_4 \delta - |\chi| \frac{3(1+\delta)}{2\sqrt{10}} + \sqrt{\lambda_1 \left[\lambda_2 + \frac{9}{40} \lambda_5 (3-\delta)(1+\delta) \right]} > 0 \quad (72b)$$

must hold $\forall \delta \in [-1, 1/3]$. In practice one finds that condition (72b), relative to the purple line, is superfluous; condition (72a), that follows from the magenta line, does matter.

Relevance of the orange line and green segment: We have randomly generated 10^6 sets of parameters $\lambda_1, \dots, \lambda_5, \chi$ and we have explicitly minimized V_4 for each of those sets. We have found that the BFB conditions obtained in this way almost coincide with the ones that one finds if, besides conditions (34a), (35), and (72), one just imposes condition (71) both on the orange line, *viz.*

$$\lambda_3 + \frac{3\lambda_4\delta}{4} - \frac{3|\chi|(1-\delta)}{\sqrt{10}} + \sqrt{\lambda_1 \left[\lambda_2 + \frac{9\lambda_5(1-\delta)^2}{10} \right]} \geq 0 \quad \forall \delta \in \left[\frac{1}{3}, 1 \right], \quad (73)$$

and on the green segment, *viz.*

$$\lambda_3 + \frac{3\lambda_4\delta}{4} - \frac{3|\chi|\sqrt{(3\delta+1)(1-\delta)}}{2\sqrt{10}} + \sqrt{\lambda_1 \left[\lambda_2 + \frac{9\lambda_5(1-\delta^2)}{10} \right]} \geq 0 \quad \forall \delta \in \left[\frac{1+2\sqrt{2}}{7}, 1 \right]. \quad (74)$$

Only seven quartic potentials were incorrectly identified as BFB in this way. This occurred because the region of sheet 3 between the red line and the green–brown line is convex, and these lines are therefore unable to correctly locate the minimum for some potentials. Our numerical analysis showed that one needs to re-scan the potentially mis-identified potentials by using 10^3 sets of parameters (δ, γ_5, η) uniformly distributed on sheet 3 between the red and green–brown lines; this additional procedure allow one to exactly reproduce the BFB V_4 ’s obtained by the direct minimization.

Procedure: Our practical procedure for checking the boundedness-from-below of V_4 consists of the following steps.

1. The necessary conditions (34a) and (35) are checked.
2. The condition (71) is tested at the special points (62).
3. Conditions (72a), (73), and (74) are enforced.
4. The selected points are scanned along the surface $Q_4 = 0$ between the red and green–brown lines.

Efficiency of the method: In order to demonstrate the efficiency of our method we have compared it with the brute-force minimization of V_4 , following the same procedure as in section 3. We randomly generated 10^6 sets of couplings $\lambda_1, \dots, \lambda_5, \chi$. Then:

- The direct minimization of the 10^6 V_4 's required 62 157 seconds and yielded 381 910 bounded from below V_4 's.
- Our proposed method¹⁶ completed the same task in 36.6 seconds, identifying exactly the same 381 910 BFB potentials.

This comparison demonstrates that our method is approximately 1 700 times faster than the brute-force minimization of V_4 .

5 Conclusions and discussion

The important findings in this work were the following:

- For the two models studied, there are *analytical* equations for the boundaries of the phase spaces. Besides the trivial equations $\epsilon = 0$ in Section 3 and $\eta = 0$ in Section 4, there are the equations

$$Q_1 = 9(1 - \delta^2) - 20\gamma_5 = 0 \quad (75)$$

in both Sections 3 and 4, and

$$Q_3 = 9(1 + \delta)^2 - 40\eta^2 = 0 \quad (76)$$

in Section 4. *Most important of all, there are equations $Q_2 = 0$ in Section 3 and $Q_4 = 0$ in Section 4*, where Q_2 and Q_4 are polynomial functions explicitly displayed in Appendix A. The latter equations have several solutions; usually, either two or three of those solutions are relevant for the boundaries of the phase spaces, while the other solutions are to be discarded.

- It is necessary to assess the convexity or concavity of the (upper) boundary of phase space in order to understand whether one must scan that surface fully, or just a few lines thereon, when studying the boundedness-from-below of the scalar potential. Namely, convex boundaries require a full scan (and the more convex they are, the more detailed that scan must be), while for concave or indefinite-concavity boundaries the scan over a few lines suffices. In order to correctly assess the convexity or concavity one must write the quartic potential as a *linear* combination of the phase-space parameters, *viz.* of δ , γ_5 , and either ϵ or η , *cf.* Eqs. (12) and (54)—and employ just those parameters—not, say, their squares—in the procedure explained in Appendix B.
- The bounded-from-below conditions on the quartic parts of the scalar potentials mostly require, in practice, numerical scans over a few *lines*—not surfaces¹⁷—at the boundary

¹⁶Since the lines in Eqs. (72)–(74) depend on the single parameter δ and are continuously differentiable, we have employed for them an efficient bisection minimization method instead of a direct scan.

¹⁷In the case in Section 4 a scan over the surface with $Q_4 = 0$ is finally needed in order to eliminate a few unbounded-from-below potentials.

of the phase space of each model.¹⁸ We have explicitly given those lines for each of the two models.

We have found, by giving random values to all the scalar fields, that the phase spaces that one obtains are the same, irrespective of whether one allows the fields to be complex—as they in general are—or one restricts all of them to be real. The reason why this is so remains to be investigated.

If the fields are taken to be real, then in both models that we have studied there are three phase-space coordinates (δ , γ_5 , and either ϵ or η) to be determined by three relative field values, *viz.* c/f , d/f , and e/f in the gauge where $a = 0$. This makes the models relatively simple, because one just needs to set one determinant equal to zero; no *ad hoc* choices of field directions are necessary. In other models that one may want to study things most likely will be more complicated—with a number of relative field values larger than the one of phase-space coordinates. This is another issue that remains to be investigated.

It must be stressed that the analytical methods that we have utilized did not dispense with the confirmation of all the results by giving random values to all the scalar fields and observing the phase spaces that get generated in this way. All our analytical phase spaces have been numerically confirmed in this way.

Usually, checking the BFB conditions through a brute-force, high-precision minimization of the quartic part of the potential demands substantial computational resources. Scanning a few conditions along the specific lines identified in our analyses accelerates the computation by several hundred times. Employing efficient minimization techniques along those lines may improve the computational performance by up to three orders of magnitude; that was a significant achievement of this work.

The expressions in Appendix A, together with computational examples in **Mathematica** notebook files, are available at <https://github.com/jurciukonis/SM-quadruplet>, enabling the reproduction of the results presented in this work.

Acknowledgements: The work of D.J. received funding from the Research Council of Lithuania (LMT) under Contract No. S-CERN-24-2. Part of the computations were performed using the infrastructure of the Lithuanian Particle Physics Consortium in the framework of the agreement No. VS-13 of Vilnius University with LMT. The work of L.L. is supported by the Portuguese Foundation for Science and Technology (FCT) through projects UIDB/00777/2020 and UIDP/00777/2020, and by the PRR (Recovery and Resilience Plan), within the scope of the investment “RE-C06-i06 - Science Plus Capacity Building”, measure “RE-C06-i06.m02 - Reinforcement of Financing for International Partnerships in Science, Technology and Innovation of the PRR,” under the project with reference 2024.01362.CERN. L.L. was furthermore supported by projects CERN/FIS-PAR/0002/2021 and CERN/FIS-PAR/0019/2021.

¹⁸We formulate the *hypothesis* that this happens because of the concave, or partly concave, nature of the relevant stretches of the boundary of phase space. When that boundary is distinctly convex—an example is displayed in Appendix C—numerical scans just over a few lines are probably not enough.

References

- [1] G. Aad *et al.* [ATLAS Collaboration], *Observation of a new particle in the search for the Standard Model Higgs boson with the ATLAS detector at the LHC*. *Phys. Lett. B* **716**, 1 (2012) [e-Print 1207.7214 [hep-ph]].
- [2] S. Chatrchyan *et al.* [CMS Collaboraton], *Observation of a New Boson at a Mass of 125 GeV with the CMS Experiment at the LHC*. *Phys. Lett. B* **716**, 30 (2012) [e-Print 1207.7235 [hep-ph]].
- [3] See S. Navas *et al.* (Particle Data Group), *Review of Particle Physics*. *Phys. Rev. D* **110**, 030001 (2024).
- [4] T. Biekötter, S. Heinemeyer, and G. Weiglein, *95.4 GeV diphoton excess at ATLAS and CMS*. *Phys. Rev. D* **109**, 035005 (2024) [e-Print: 2306.03889 [hep-ph]].
- [5] S. Bhattacharya, B. Lieberman, M. Kumar, A. Crivellin, Y. Fang, R. Mazini, and B. Mellado, *Emerging Excess Consistent with a Narrow Resonance at 152 GeV in High-Energy Proton–Proton Collisions*. E-Print: 2503.16245 [hep-ph].
- [6] A. Arhrib, R. Benbrik, M. Chabab, G. Moultaka, M. C. Peyranère, L. Rahili, and J. Ramadan, *The Higgs Potential in the Type II Seesaw Model*. *Phys. Rev. D* **84**, 095005 (2011) [e-Print: 1105.1925 [hep-ph]].
- [7] C. Bonilla, R. M. Fonseca, and J. W. F. Valle, *Consistency of the triplet seesaw model revisited*. *Phys. Rev. D* **92**, 075028 (2015) [e-Print: 1508.02323 [hep-ph]].
- [8] G. Moultaka and M. C. Peyranère, *Vacuum stability conditions for Higgs potentials with $SU(2)_L$ triplets*. *Phys. Rev. D* **103**, 115006 (2021) [e-Print: 2012.13947 [hep-ph]].
- [9] B. Dirgantara, K. Kannike and W. Sreethawong, *Vacuum stability and radiative symmetry breaking of the scale-invariant singlet extension of type II seesaw model*. *Eur. Phys. J. C* **83**, 253 (2023) [e-Print: 2301.00487 [hep-ph]].
- [10] K. Kannike, *Constraining the Higgs trilinear coupling from an $SU(2)$ quadruplet with bounded-from-below conditions*. *J. High Energ. Phys.* **2024**, 176 (2024) [e-Print: 2311.17995 [hep-ph]].
- [11] S. Kanemura, M. Kikuchi and K. Yagyu, *Probing exotic Higgs sectors from the precise measurement of Higgs boson couplings*. *Phys. Rev. D* **88**, 015020 (2013) [e-Print: 1301.7303 [hep-ph]].
- [12] C. W. Chiang and K. Yagyu, *Models with higher weak-isospin Higgs multiplets*. *Phys. Lett. B* **786**, 268 (2018) [e-Print: 1808.10152 [hep-ph]].
- [13] J. Hisano and K. Tsumura, *Higgs boson mixes with an $SU(2)$ septet representation*. *Phys. Rev. D* **87**, 053004 (2013) [e-Print: 1301.6455 [hep-ph]].

- [14] D. Jurčiukonis and L. Lavoura, *On the Addition of a Large Scalar Multiplet to the Standard Model*. *Prog. Theor. Exp. Phys.* **2024**, 083B06 (2024) [e-Print: 2404.07897 [hep-ph]].
- [15] A. Giannetti, J. Herrero-García, S. Marciano, D. Meloni, and D. Vatsyayan, *Neutrino masses from new seesaw models: low-scale variants and phenomenological implications*. *Eur. Phys. J. C* **84**, 803 (2024) [e-Print: 2312.14119 [hep-ph]].
- [16] A. Giannetti, J. Herrero-García, S. Marciano, D. Meloni, and D. Vatsyayan, *Neutrino masses from new Weinberg-like operators: phenomenology of TeV scalar multiplets*. *J. High Energ. Phys.* **2024**, 055 (2024) [e-Print: 2312.13356 [hep-ph]].
- [17] M. Abud and G. Sartori, *The Geometry of Orbit Space and Natural Minima of Higgs Potentials*. *Phys. Lett. B* **104**, 147 (1981).
- [18] J. S. Kim, *Orbit Spaces of Low Dimensional Representations of Simple Compact Connected Lie Groups and Extrema of a Group Invariant Scalar Potential*. *J. Math. Phys.* **25**, 1694 (1984).
- [19] A. Costantini, M. Ghezzi, and G. M. Pruna, *Theoretical constraints on the Higgs potential of the general 331 model*. *Phys. Lett. B* **808**, 135638 (2020) [e-Print: 2001.08550 [hep-ph]].
- [20] M. Heikinheimo, K. Kannike, F. Lyonnet, M. Raidal, K. Tuominen, and H. Veermäe, *Vacuum Stability and Perturbativity of $SU(3)$ Scalars*. *J. High Energ. Phys.* **2017**, 014 (2017) [e-Print: 1707.08980 [hep-ph]].
- [21] A. Milagre, D. Jurčiukonis, and L. Lavoura, *Vacuum stability conditions for new $SU(2)$ multiplets*. *Prog. Theor. Exp. Phys.* **2025**, 093B01 (2025) [e-Print: 2505.05272 [hep-ph]].
- [22] K. Kannike, *Vacuum stability conditions from copositivity criteria*. *Eur. Phys. J. C* **72**, 2093 (2012) [e-Print: 1205.3781 [hep-ph]].
- [23] G. Ulrich and L. T. Watson, *Positivity Conditions for Quartic Polynomials*. *SIAM J. Sci. Comput.* **15**, 528 (1994).

A The expressions of Q_2 and Q_4

Q_2 : For the quantity Q_2 in Eq. (22) one has

$$Q_2 = \sum_{n=0}^6 b_n (10\gamma_5)^n. \quad (\text{A1})$$

The coefficients b_0, \dots, b_6 are functions of δ and ϵ^2 :

$$b_0 = 3^8 [(1 + \delta)^3 - 8\epsilon^2]^2 \left[(127 + 225\delta + 405\delta^2 + 243\delta^3)^2 \right. \quad (\text{A2a})$$

$$\left. - 4(28795 + 164619\delta + 281070\delta^2 + 253206\delta^3 + 185895\delta^4 + 98415\delta^5) \epsilon^2 \right] \quad (\text{A2b})$$

$$+ 12(49331 + 167724\delta + 174546\delta^2 + 65772\delta^3 + 54675\delta^4) \epsilon^4 \quad (\text{A2c})$$

$$\left. - 4096(292 + 585\delta + 54\delta^2 + 81\delta^3) \epsilon^6 + 1048576\epsilon^8 \right], \quad (\text{A2d})$$

$$b_1 = -2 \times 3^6 [(1 + \delta)^3 (127 + 225\delta + 405\delta^2 + 243\delta^3) (1129 \quad (\text{A3a})$$

$$+ 2868\delta + 4614\delta^2 + 3348\delta^3 + 729\delta^4) \quad (\text{A3b})$$

$$- 8(241961 + 1921725\delta + 6748761\delta^2 + 14553795\delta^3 + 20815167\delta^4 \quad (\text{A3c})$$

$$+ 20846649\delta^5 + 14579811\delta^6 + 6344001\delta^7 + 1303452\delta^8 + 39366\delta^9) \epsilon^2 \quad (\text{A3d})$$

$$+ 4(3673191 + 24261588\delta + 77591040\delta^2 + 128209796\delta^3 + 127686438\delta^4 \quad (\text{A3e})$$

$$+ 86310396\delta^5 + 40192344\delta^6 + 8427564\delta^7 - 639333\delta^8) \epsilon^4 \quad (\text{A3f})$$

$$- 16(3786799 + 23774769\delta + 51666021\delta^2 + 56099983\delta^3 + 33353169\delta^4 \quad (\text{A3g})$$

$$+ 14415495\delta^5 + 2899899\delta^6 - 372519\delta^7) \epsilon^6 \quad (\text{A3h})$$

$$+ 512(350855 + 1404999\delta + 1906131\delta^2 + 844173\delta^3 + 304122\delta^4 \quad (\text{A3i})$$

$$+ 43680\delta^5 - 6624\delta^6) \epsilon^8 \quad (\text{A3j})$$

$$- 262144(1041 + 2439\delta + 546\delta^2 + 164\delta^3) \epsilon^{10} + 201326592\epsilon^{12}], \quad (\text{A3k})$$

$$b_2 = 3^4 [1998033 + 10659240\delta + 31114620\delta^2 + 58455512\delta^3 + 75085254\delta^4 \quad (\text{A4a})$$

$$+ 65745432\delta^5 + 37096380\delta^6 + 12159720\delta^7 + 1791153\delta^8 \quad (\text{A4b})$$

$$- 12(1405269 + 10375407\delta + 27924145\delta^2 + 45055699\delta^3 + 45386607\delta^4 \quad (\text{A4c})$$

$$+ 28978749\delta^5 + 10862667\delta^6 + 1709505\delta^7) \epsilon^2 \quad (\text{A4d})$$

$$+ 4(26754009 + 143143614\delta + 389331183\delta^2 + 492368452\delta^3 + 327588327\delta^4 \quad (\text{A4e})$$

$$+ 112833054\delta^5 + 23517297\delta^6) \epsilon^4 \quad (\text{A4f})$$

$$- 64(4988475 + 29262861\delta + 54167994\delta^2 + 46168094\delta^3 \quad (\text{A4g})$$

$$+ 12881115\delta^4 + 2068389\delta^5) \epsilon^6 \quad (\text{A4h})$$

$$+ 1536(524649 + 1964682\delta + 2513849\delta^2 + 517512\delta^3 + 33072\delta^4) \epsilon^8 \quad (\text{A4i})$$

$$- 262144(4056 + 10269\delta + 1200\delta^2 - 32\delta^3) \epsilon^{10} + 805306368\epsilon^{12}], \quad (\text{A4j})$$

$$b_3 = -2^5 \times 3^2 [219\,250 + 6\delta (133\,498 + 288\,469\delta + 369\,420\delta^2) \quad (A5a)$$

$$+ 298\,701\delta^3 + 139\,482\delta^4 + 25\,515\delta^5) \quad (A5b)$$

$$- 2 (573\,229 + 3\,817\,557\delta + 7\,002\,354\delta^2 + 7\,473\,690\delta^3) \quad (A5c)$$

$$+ 4\,385\,745\delta^4 + 1\,289\,601\delta^5) \epsilon^2 \quad (A5d)$$

$$+ (6\,285\,479 + 23\,724\,876\delta + 49\,111\,578\delta^2 + 39\,010\,284\delta^3 + 14\,624\,631\delta^4) \epsilon^4 \quad (A5e)$$

$$- 2 (6\,247\,069 + 29\,947\,395\delta + 37\,835\,679\delta^2 + 24\,267\,897\delta^3) \epsilon^6 \quad (A5f)$$

$$+ 32 (752\,119 + 2\,076\,849\delta + 2\,461\,170\delta^2) \epsilon^8 - 16\,384 (1\,316 + 3\,621\delta) \epsilon^{10} \quad (A5g)$$

$$+ 16\,777\,216\epsilon^{12}] , \quad (A5h)$$

$$b_4 = 2^8 [52\,006 + 18\delta (6\,428 + 9\,618\delta + 6\,588\delta^2 + 2\,187\delta^3) \quad (A6a)$$

$$- 4 (37\,645 + 222\,291\delta + 212\,463\delta^2 + 105\,705\delta^3) \epsilon^2 \quad (A6b)$$

$$+ 48 (14\,963 + 30\,762\delta + 38\,871\delta^2) \epsilon^4 \quad (A6c)$$

$$- 28 (28\,411 + 88\,407\delta) \epsilon^6 + 1\,024\,009\epsilon^8] , \quad (A6d)$$

$$b_5 = -2^{13} [2 (89 + 90\delta + 81\delta^2) - 2 (103 + 531\delta) \epsilon^2 + 811\epsilon^4] , \quad (A7)$$

$$b_6 = 2^{16}. \quad (A8)$$

Q4: For the quantity Q_4 in Eq. (61) one has

$$Q_4 = \sum_{n=0}^6 d_n \gamma_5^n. \quad (A9)$$

The coefficients d_0, \dots, d_6 are functions of δ and η^2 :

$$d_0 = \eta^4 [104\,976R^4 + 3\,732\,480 (7 - 10\delta - \delta^2) \eta^2 + 33\,177\,600 \eta^4] , \quad (A10)$$

$$d_1 = -\eta^2 [52\,488R^5S + 466\,560R (84 - 61\delta - 38\delta^2 - 5\delta^3) \eta^2 \quad (A11a)$$

$$+ 8\,294\,400 (29 - 19\delta - 4\delta^2) \eta^4 + 147\,456\,000 \eta^6] , \quad (A11b)$$

$$d_2 = 6\,561R^6S^2 + 29\,160R^2 (513 + 48\delta - 400\delta^2 - 76\delta^3 - 13\delta^4) \eta^2 \quad (A12a)$$

$$+ 259\,200 (2\,241 - 1\,474\delta - 785\delta^2 + 160\delta^3 + 30\delta^4) \eta^4 \quad (A12b)$$

$$+ 4\,608\,000 (149 - 36\delta - 14\delta^2) \eta^6 + 163\,840\,000 \eta^8 , \quad (A12c)$$

$$d_3 = -14580R^3S(117 - 6\delta - 59\delta^2) \quad (A13a)$$

$$-64800(8253 - 3378\delta - 5260\delta^2 + 1202\delta^3 + 463\delta^4)\eta^2 \quad (A13b)$$

$$-576000(2116 - 623\delta - 487\delta^2)\eta^4 - 624640000\eta^6, \quad (A13c)$$

$$d_4 = 900[9(20601 - 1404\delta - 18378\delta^2 + 2756\delta^3 + 3225\delta^4) \quad (A14a)$$

$$+80(13119 - 2770\delta - 4945\delta^2)\eta^2 + 1025600\eta^4], \quad (A14b)$$

$$d_5 = -2^{11} \times 5^3 [9(117 - 6\delta - 59\delta^2) + 2440\eta^2], \quad (A15)$$

$$d_6 = 2^{18} \times 5^4. \quad (A16)$$

Here,

$$R = 3 - \delta, \quad (A17a)$$

$$S = 1 + \delta. \quad (A17b)$$

B Concavity or convexity of the phase-space boundary

If a surface is the topological boundary of a set of points in three dimensions, then that surface is said to be concave (or ‘concave up’) at a point if it bends toward the outer-pointing surface normal at that point; the surface is convex (or ‘concave down’) if it bends away from the outer-pointing normal.

Let $z = f(x, y)$ represent the surface bounding *above* a volume in (x, y, z) space. Then the local concavity is characterized by the definiteness of the Hessian matrix

$$H = \begin{pmatrix} \frac{\partial^2 f}{\partial x^2} & \frac{\partial^2 f}{\partial x \partial y} \\ \frac{\partial^2 f}{\partial x \partial y} & \frac{\partial^2 f}{\partial y^2} \end{pmatrix} := \begin{pmatrix} f_{xx} & f_{xy} \\ f_{xy} & f_{yy} \end{pmatrix}. \quad (\text{B1})$$

- The surface is locally concave if the Hessian is positive semidefinite, *viz.* if $\det H \geq 0$, $f_{xx} \geq 0$, and $f_{yy} \geq 0$.
- The surface is locally convex if the Hessian is negative semidefinite, *viz.* if $\det H \geq 0$, $f_{xx} \leq 0$, and $f_{yy} \leq 0$.
- The surface is neither concave nor convex if the Hessian is indefinite,¹⁹ *viz.* if $\det H \leq 0$.

The boundary between regions of definite concavity (either concave up or concave down) and indefinite concavity may be found by solving the equation $\det H = 0$.

In our specific cases, the concave and convex regions of the surface bounding the phase space from above may be identified by scanning the surface over the parameters δ and γ_5 and using the following procedure:

1. Obtain analytical solutions of $Q_i = 0$ for $i = 2, 4, 5$, with respect to the relevant parameters—either ϵ , η , or ε , respectively.
2. Determine which of the solutions corresponds to the surface at the given point.
3. Compute the Hessian matrix at that point by double-differentiating the relevant solution with respect to δ and γ_5 .
4. Evaluate the concavity conditions at the given point, *viz.* determine the signs of $\det H$, f_{xx} , and f_{yy} .

¹⁹In this case, the surface may be concave in one direction but convex in another direction at the same point.

C One further case

Potential: If the doublet Φ and the quadruplet Ξ have the same hypercharge and if there is no symmetry under $\Xi \rightarrow -\Xi$, then in general

$$V_{4,\text{extra}} = \frac{\chi}{2} T_1^\dagger T_2 + \frac{\nu}{2} T_3^\dagger T_1 + \frac{\iota}{2} T_3^\dagger T_2 + \text{H.c.}, \quad (\text{C1})$$

where T_1 is the $SU(2)$ triplet in Eq. (47), T_2 is the $SU(2)$ triplet in Eq. (48), and

$$T_3 = (\Xi \otimes \Phi)_{\mathbf{3}} = \frac{1}{2} \begin{pmatrix} \sqrt{3}bc - ad \\ \sqrt{2}(bd - ae) \\ be - \sqrt{3}af \end{pmatrix} \quad (\text{C2})$$

is one further $SU(2)$ triplet. In this Appendix we follow Ref. [10] and assume $\chi = \iota = 0$, even if this is inconsistent because there is no symmetry that enforces this and therefore nonzero χ and ι are needed for renormalization.

Parameter ε : The dimensionless parameter

$$\varepsilon \equiv \frac{|T_3^\dagger T_1|}{\sqrt{F_1^3 F_2}} \quad (\text{C3})$$

is non-negative by definition. Then (with $\chi = \iota = 0$),

$$V_{4,\text{extra}} = |\nu| \varepsilon \sqrt{F_1^3 F_2} \cos(\arg \nu + \arg T_3^\dagger T_1), \quad (\text{C4})$$

so that

$$\frac{V_4}{F_2^2} = \frac{\lambda_1}{2} (\sqrt{r})^4 + |\nu| \varepsilon \cos(\arg \nu + \arg T_3^\dagger T_1) (\sqrt{r})^3 + \left(\lambda_3 + \frac{3}{4} \lambda_4 \delta \right) (\sqrt{r})^2 + \frac{\lambda_2 + 2\lambda_5 \gamma_5}{2}. \quad (\text{C5})$$

Gauge $a = 0$: In the gauge where $a = 0$ throughout space-time, $T_3^\dagger T_1 = (F_1/2)be^*$ and therefore

$$\varepsilon^2 = \frac{E}{4(F + E + D + C)}. \quad (\text{C6})$$

From Eqs. (5b) and (C6) we note that

$$3(1 + \delta) - 16\varepsilon^2 = \frac{6F + 2D}{F + E + D + C}, \quad (\text{C7a})$$

$$3(1 - \delta) - 8\varepsilon^2 = \frac{6C + 4D}{F + E + D + C} \quad (\text{C7b})$$

are both non-negative. There are thus two upper bounds on ε^2 :

$$\varepsilon^2 \leq \frac{3(1 + \delta)}{16}, \quad (\text{C8a})$$

$$\varepsilon^2 \leq \frac{3(1 - \delta)}{8}. \quad (\text{C8b})$$

It follows from them that the maximum possible value of ε^2 is $1/4$ and that it is attained when $\delta = 1/3$, *viz.* at the point that we shall call \widehat{P}_3 in Eq. (C21c).

Boundary: Using Eqs. (19) and

$$\varepsilon^2 = \frac{z^2}{4}, \quad (\text{C9})$$

we write the condition

$$\det \begin{pmatrix} \frac{\partial \delta}{\partial x} & \frac{\partial \delta}{\partial y} & \frac{\partial \delta}{\partial z} \\ \frac{\partial \gamma_5}{\partial x} & \frac{\partial \gamma_5}{\partial y} & \frac{\partial \gamma_5}{\partial z} \\ \frac{\partial \varepsilon^2}{\partial x} & \frac{\partial \varepsilon^2}{\partial y} & \frac{\partial \varepsilon^2}{\partial z} \end{pmatrix} = 0. \quad (\text{C10})$$

We therefrom obtain

$$\varepsilon^2 Q_1 Q_5 = 0, \quad (\text{C11})$$

where Q_1 is the quantity defined in Eq. (4) and

$$Q_5 = \sum_{n=0}^6 e_n (10\gamma_5)^n. \quad (\text{C12})$$

The coefficients e_0, \dots, e_6 are functions of δ and ε^2 . Defining

$$\tilde{R} = \delta - 1, \quad (\text{C13a})$$

$$\tilde{S} = 9\delta + 7, \quad (\text{C13b})$$

one has

$$e_0 = -3^6 \left[3\tilde{R}(\delta+1)^2 + 32\varepsilon^2 \right]^2 \left[81\tilde{R}^2\tilde{S}^4 + 432\tilde{R}\tilde{S}^2(7\delta+9)(21-5\delta)\varepsilon^2 \right. \quad (\text{C14a})$$

$$\left. + 576(56841 + 81820\delta + 10998\delta^2 - 52452\delta^3 - 31671\delta^4)\varepsilon^4 \right. \quad (\text{C14b})$$

$$\left. - 2^{18} \times 3(172 + 183\delta - 18\delta^2 - 81\delta^3)\varepsilon^6 + 2^{28}\varepsilon^8 \right], \quad (\text{C14c})$$

$$e_1 = 2 \times 3^5 \left[243\tilde{R}^3\tilde{S}^3(1+\delta)^2(39+66\delta+23\delta^2) \right. \quad (\text{C15a})$$

$$\left. + 2592\tilde{R}^2\tilde{S}(6209+26546\delta+40720\delta^2+24272\delta^3) \right. \quad (\text{C15b})$$

$$\left. + 1773\delta^4 - 1674\delta^5 + 458\delta^6 \right) \varepsilon^2 \quad (\text{C15c})$$

$$\left. + 1728\tilde{R}(975729+3617501\delta+4193369\delta^2+606141\delta^3) \right. \quad (\text{C15d})$$

$$\left. - 1803301\delta^4 - 995505\delta^5 - 223269\delta^6 - 79209\delta^7 \right) \varepsilon^4 \quad (\text{C15e})$$

$$\left. + 9216(1506843+2982015\delta+68969\delta^2-2724639\delta^3) \right. \quad (\text{C15f})$$

$$\left. - 1269563\delta^4 + 330409\delta^5 + 203799\delta^6 - 49257\delta^7 \right) \varepsilon^6 \quad (\text{C15g})$$

$$\left. - 2^{17} \times 3(171715+238925\delta-8745\delta^2) \right. \quad (\text{C15h})$$

$$\left. - 146049\delta^3 - 38502\delta^4 + 14560\delta^5 - 6624\delta^6 \right) \varepsilon^8 \quad (\text{C15i})$$

$$\left. + 2^{28}(717+637\delta-182\delta^2-164\delta^3)\varepsilon^{10} - 2^{38}\varepsilon^{12} \right], \quad (\text{C15j})$$

$$e_2 = 3^3 \left[243 \tilde{R}^2 \tilde{S}^2 (2481 + 8220\delta + 9350\delta^2 + 4060\delta^3 + 465\delta^4) \right] \quad (C16a)$$

$$+ 1296 \tilde{R} (640633 + 2533410\delta + 3215487\delta^2 + 812348\delta^3) \quad (C16b)$$

$$- 927001\delta^4 - 202494\delta^5 + 219073\delta^6) \varepsilon^2 \quad (C16c)$$

$$+ 1728 (6014521 + 13113034\delta + 940951\delta^2 - 11539124\delta^3) \quad (C16d)$$

$$- 3255977\delta^4 + 1511370\delta^5 - 493319\delta^6) \varepsilon^4 \quad (C16e)$$

$$- 2^{12} \times 3^2 (1990309 + 3074189\delta - 369486\delta^2) \quad (C16f)$$

$$- 1636950\delta^3 - 91351\delta^4 + 211785\delta^5) \varepsilon^6 \quad (C16g)$$

$$+ 2^{17} \times 3 (790995 + 797218\delta - 103565\delta^2 - 178168\delta^3 + 73616\delta^4) \varepsilon^8 \quad (C16h)$$

$$- 2^{28} (2904 + 2051\delta - 400\delta^2 + 32\delta^3) \varepsilon^{10} + 2^{40} \varepsilon^{12} \right], \quad (C16i)$$

$$e_3 = 2^6 \left[729 \tilde{R} \tilde{S} (641 + 1820\delta + 1510\delta^2 + 220\delta^3 - 95\delta^4) \right] \quad (C17a)$$

$$+ 972 (74101 + 171935\delta + 26162\delta^2) \quad (C17b)$$

$$- 148706\delta^3 - 36503\delta^4 + 44083\delta^5) \varepsilon^2 \quad (C17c)$$

$$- 648 (1097753 + 1761596\delta - 156618\delta^2 - 756868\delta^3 + 118521\delta^4) \varepsilon^4 \quad (C17d)$$

$$+ 1728 (2284741 + 2537353\delta - 580705\delta^2 - 622573\delta^3) \varepsilon^6 \quad (C17e)$$

$$- 2^{12} \times 3^2 (362107 + 203059\delta - 58878\delta^2) \varepsilon^8 \quad (C17f)$$

$$+ 2^{23} \times 3 (980 + 491\delta) \varepsilon^{10} - 2^{35} \varepsilon^{12} \right], \quad (C17g)$$

$$e_4 = 2^9 [81 (723 + 1620\delta + 530\delta^2 - 620\delta^3 - 205\delta^4) \quad (C18a)$$

$$- 216 (4331 + 7303\delta - 271\delta^2 - 3683\delta^3) \varepsilon^2 \quad (C18b)$$

$$+ 1152 (5757 + 5450\delta - 1295\delta^2) \varepsilon^4 \quad (C18c)$$

$$- 1152 (19977 + 14623\delta) \varepsilon^6 + 49280128\varepsilon^8], \quad (C18d)$$

$$e_5 = -2^{14} [135 + 162\delta - 9\delta^2 - (1236 + 1356\delta) \varepsilon^2 + 5224\varepsilon^4], \quad (C19)$$

$$e_6 = 2^{16}. \quad (C20)$$

It follows from Eq. (C11) that the border of the $(\delta, \gamma_5, \varepsilon)$ phase space has three sheets:

1. Sheet 1 has equation $Q_1 = 0$.

2. Sheet 2 has equation $\varepsilon = 0$.

3. Sheet 3 has equation $Q_5 = 0$.

It should be emphasized that the equation $Q_5 = 0$ usually yields up to six real solutions for ε^2 , for any given values of δ and γ_5 . (That equation may also have non-real solutions.) However, not all of those solutions form the border of phase space. That border must be confirmed by giving random (in general, complex) values to the fields c , d , e , and f and explicitly constructing the phase space via Eqs. (3c), (5b), and (C6).

Points: We define the points

$$\widehat{P}_1 : \quad \delta = -1, \quad \gamma_5 = \varepsilon = 0; \quad (\text{C21a})$$

$$\widehat{P}_2 : \quad \delta = 1, \quad \gamma_5 = \varepsilon = 0; \quad (\text{C21b})$$

$$\widehat{P}_3 : \quad \delta = \frac{1}{3}, \quad \gamma_5 = \frac{2}{5}, \quad \varepsilon = \frac{1}{2}; \quad (\text{C21c})$$

$$\widehat{P}_4 : \quad \delta = \frac{1}{3}, \quad \gamma_5 = 0, \quad \varepsilon = \frac{1}{3}; \quad (\text{C21d})$$

$$\widehat{P}_5 : \quad \delta = \frac{1}{9}, \quad \gamma_5 = \frac{2}{5}, \quad \varepsilon = 0. \quad (\text{C21e})$$

Points \widehat{P}_1 and \widehat{P}_2 have $Q_1 = \varepsilon = Q_5 = 0$. Point \widehat{P}_3 has $Q_1 = Q_5 = 0$ but $\varepsilon \neq 0$. Point \widehat{P}_5 has $\varepsilon = Q_5 = 0$ but $Q_1 \neq 0$. Point \widehat{P}_4 is solely on sheet 3.

Main lines: We define three lines connecting point \widehat{P}_1 to point \widehat{P}_2 :

- The blue line has $Q_1 = \varepsilon = 0$.
- The purple line has $\varepsilon = Q_5 = 0$; this gives

$$\gamma_5 = \begin{cases} \frac{9(1+\delta)^2}{10} & \Leftarrow -1 \leq \delta \leq -\frac{3}{5}, \\ -\frac{9\tilde{R}\tilde{S}}{160} & \Leftarrow -\frac{3}{5} \leq \delta \leq 1. \end{cases} \quad (\text{C22})$$

Point \widehat{P}_5 is on the purple line.

- The magenta–brown line has $Q_1 = Q_5 = 0$. It has two segments, the magenta one from \widehat{P}_1 to \widehat{P}_3 and the brown one from \widehat{P}_3 to \widehat{P}_2 . Both segments have $\gamma_5 = 9(1-\delta^2)/20$; the magenta segment has

$$\varepsilon^2 = \frac{3(1+\delta)}{16}, \quad (\text{C23})$$

while the brown segment has

$$\varepsilon^2 = \frac{3 \left[27 + 36\delta - 142\delta^2 + 68\delta^3 + 11\delta^4 + \sqrt{-\tilde{R}^5 (23\delta + 9)^3} \right]}{16384\delta^3}. \quad (\text{C24})$$

At their meeting point \widehat{P}_3 the magenta and brown segments have derivatives $d\varepsilon^2/d\delta$ of opposite sign. Notice that the magenta segment materializes the upper bound (C8a) on ε^2 .

Bounding surface: The surface bounding phase space has the topology of the surface of a sphere. On that sphere lie the two points \widehat{P}_1 and \widehat{P}_2 connected by the blue line, the purple line, and the magenta–brown line. Sheet 1 connects the magenta–brown line to the blue line, then sheet 2 links the blue line to the purple line, and finally sheet 3 goes from the purple line to the magenta–brown line.

Yellow line: The yellow line is on sheet 3. It is the line where the bounding surface has minimal $\gamma_5 = 0$. Setting $\gamma_5 = Q_5 = 0$ one obtains

$$\varepsilon^2 = \frac{3(1-\delta^2)(1+\delta)}{32}, \quad (\text{C25})$$

which defines the yellow line together with $\gamma_5 = 0$. That line connects \hat{P}_1 to \hat{P}_2 just as the main lines. It attains maximum $\varepsilon = 1/3$ when $\delta = 1/3$.

Red line: This line connects \hat{P}_3 to \hat{P}_4 and then proceeds to \hat{P}_5 through the equations

$$\delta = \frac{3 - 11\varepsilon^2 + 5\sqrt{\varepsilon^2(24 - 47\varepsilon^2)}}{27}, \quad (\text{C26a})$$

$$\gamma_5 = \frac{54 - 504\varepsilon^2 + 2359\varepsilon^4 - \sqrt{\varepsilon^2(24 - 47\varepsilon^2)^3}}{135}. \quad (\text{C26b})$$

Between \hat{P}_3 and \hat{P}_4 this line gives, for each γ_5 , the point of maximum ε .

Orange line: This line is on sheet 3 and materializes the upper bound (C8b). It goes from \hat{P}_2 to \hat{P}_3 and is given by

$$\gamma_5 = \frac{9(1-\delta)^2}{10}, \quad (\text{C27a})$$

$$\varepsilon^2 = \frac{3(1-\delta)}{8}. \quad (\text{C27b})$$

Figures: Figure 5 displays two perspectives of phase space. Unfortunately, on those per-

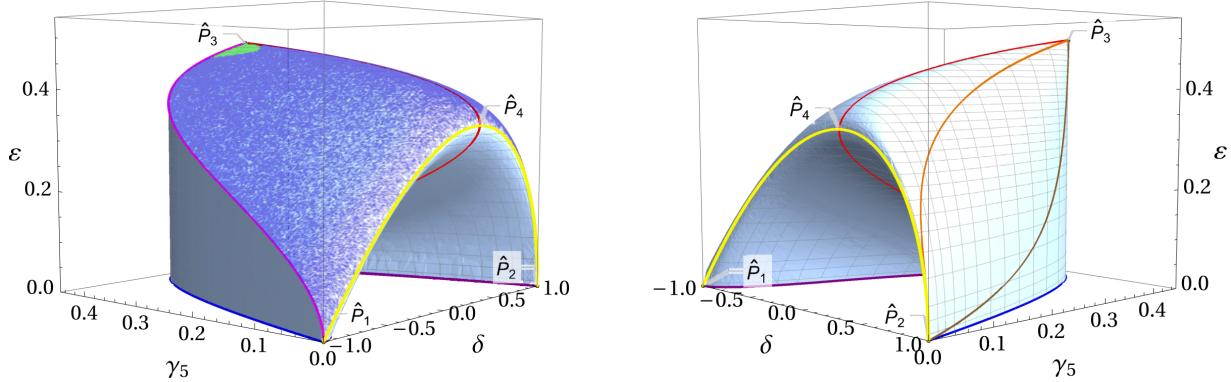


Figure 5: Two perspectives of the boundary of phase space. The points and lines displayed are defined in the text. The blue points in left panel indicate the convex part of the surface $Q_5 = 0$; green points correspond to the part of that surface that is neither concave nor convex.

spectives the purple line is barely visible and point \hat{P}_5 is not visible at all, therefore Fig. 6 shows the projection of phase space on the γ_5 vs. δ plan.

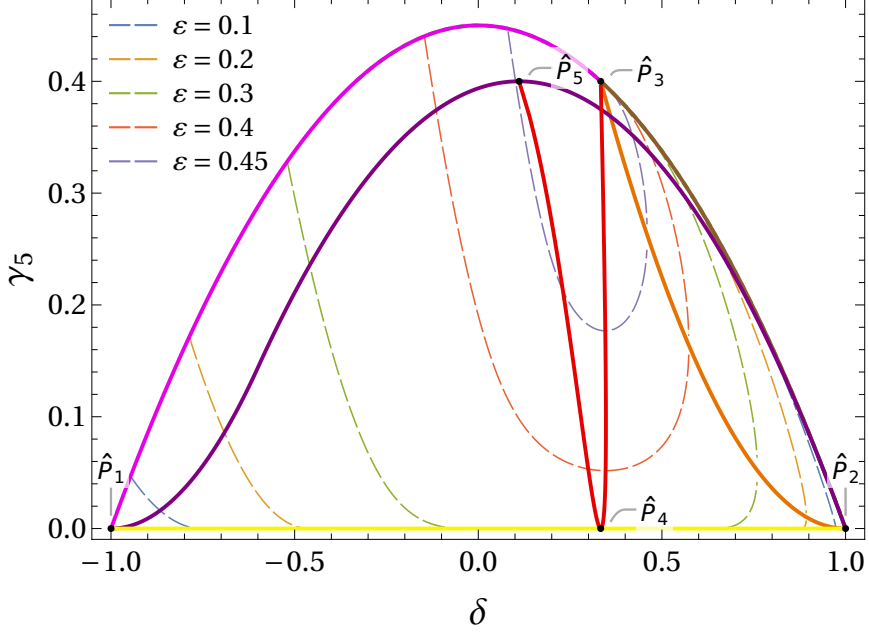


Figure 6: The projection of phase space on the γ_5 vs. δ plane. The points and lines displayed are defined in the text. The blue line coincides with the magenta–brown line in this projection. The iso-lines of constant ε on the upper part of sheet 3—the part of that sheet that connects the yellow line to the magenta–brown line—are marked by dashed lines in various colours.

Convexity of sheet 3: The upward-facing part of sheet 3, *i.e.* the one with maximum ε , is almost entirely convex, except for a small region near the sheet’s top that is neither concave nor convex, illustrated by the green area in Fig. 5. The red line lies close to, but outside, this green region.

Boundedness-from-below: The potential in Eq. (C5) is similar to the one in Eq. (12), so the BFB conditions (42)–(44) once again hold, just as the necessary BFB conditions (34a), (35), and (40); one must also discard all the situations where conditions (41) hold true. Of course, in the second Eq. (33) one must make $\xi \rightarrow \nu$ and $\epsilon \rightarrow \varepsilon$.

Relevance of the lines: We have randomly generated 10^6 sets of parameters $\lambda_1, \dots, \lambda_5, \nu$, and we have explicitly minimized V_4 for each of these sets. We have found that by applying conditions (42)–(44) just along the *magenta, red, yellow, and orange lines* allows one to discard the majority (up to 99.95%) of the potentials that are not bounded from below. In order to achieve exact agreement with the results of the minimization of V_4 , the selected parameter sets should be re-evaluated by applying conditions (42)–(44) for every possible $(\delta, \gamma_5, \varepsilon)$ on the upper part of sheet 3. Since the convexity of phase space is stronger than in the case $Y = 1/2$ with reflection symmetry, a larger number of points must be used for the

scan; we have used 10^5 points $(\delta, \gamma_5, \varepsilon)$.²⁰

Procedure: Our practical recommendation for establishing the boundedness-from-below of V_4 consists of the following steps.

1. The necessary conditions (34a), (35), and (40) are checked.
2. Cases satisfying conditions (41) are discarded.
3. Conditions (42)–(44) are tested for \aleph and \beth defined through Eqs. (39) at the special points (C21).²¹
4. Conditions (42)–(44) are tested for \aleph and \beth defined along the magenta, red, yellow, and orange lines.
5. For full precision, the remaining points must be scanned through 10^5 points uniformly distributed over the whole upper part of surface $Q_5 = 0$.

²⁰An alternative approach would be to firstly minimize the quantity Δ in Eq. (38a) over the upper part of sheet 3, then to discard the points where Δ is negative, and finally to apply condition (37).

²¹It is worth noting that steps 1 and 2 by themselves alone allow the elimination of up to 91.45% of the potentials violating the BFB conditions. Complemented with the scan over the special points, up to 97.76% of the potentials violating the BFB conditions are discarded.

D Unitarity conditions

For the model in Section 3, *viz.* for the quartic potential given by Eqs. (6) and (8), the unitarity conditions are

$$|\lambda_1| < M, \quad (\text{D1a})$$

$$|\lambda_2| < M, \quad (\text{D1b})$$

$$|\lambda_2 + 2\lambda_5| < M, \quad (\text{D1c})$$

$$\left| \lambda_2 + \frac{3\lambda_5}{5} \right| < M, \quad (\text{D1d})$$

$$\left| \lambda_2 + \frac{9\lambda_5}{5} \right| < M, \quad (\text{D1e})$$

$$|\lambda_3| + \frac{3}{4} |\lambda_4| < M, \quad (\text{D1f})$$

$$\left| \lambda_3 - \frac{5\lambda_4}{4} \right| < M, \quad (\text{D1g})$$

$$|3\lambda_1 + 5\lambda_2 + 3\lambda_5| + \sqrt{(3\lambda_1 - 5\lambda_2 - 3\lambda_5)^2 + 32\lambda_3^2} < 2M, \quad (\text{D1h})$$

$$\left| \lambda_1 + \lambda_2 - \frac{11}{5}\lambda_5 \right| + \sqrt{\left(\lambda_1 - \lambda_2 + \frac{11}{5}\lambda_5 \right)^2 + 10\lambda_4^2} < 2M, \quad (\text{D1i})$$

$$\left| \lambda_1 + \lambda_3 + \frac{5}{4}\lambda_4 \right| + \sqrt{\left(\lambda_1 - \lambda_3 - \frac{5}{4}\lambda_4 \right)^2 + 24|\xi|^2} < 2M. \quad (\text{D1j})$$

For the model in Section 4, *viz.* for the quartic potential given by Eqs. (6) and (51), the unitarity conditions are conditions (D1a), (D1b), (D1d), (D1e), (D1h), (D1i), and

$$\left| \lambda_3 + \frac{3\lambda_4}{4} \right| < M, \quad (\text{D2a})$$

$$\left| \lambda_3 - \frac{3\lambda_4}{4} \right| + \frac{3}{\sqrt{10}} |\chi| < M, \quad (\text{D2b})$$

$$\left| \lambda_3 - \frac{5\lambda_4}{4} \right| < M, \quad (\text{D2c})$$

$$\left| \lambda_3 + \frac{5\lambda_4}{4} \right| + \sqrt{\frac{5}{2}} |\chi| < M, \quad (\text{D2d})$$

$$|\lambda_1 + \lambda_2 + 2\lambda_5| + \sqrt{(\lambda_1 - \lambda_2 - 2\lambda_5)^2 + 4|\chi|^2} < 2M. \quad (\text{D2e})$$

For the model in Appendix C, *viz.* for the quartic potential given by Eqs. (6) and (C1), the unitarity conditions are conditions (D1a)–(D1f), (D1h), and

$$\left| \lambda_3 + \frac{5\lambda_4}{4} \right| < M, \quad (\text{D3a})$$

$$\left| \lambda_1 + \lambda_3 - \frac{5}{4}\lambda_4 \right| + \sqrt{\left(\lambda_1 - \lambda_3 + \frac{5}{4}\lambda_4 \right)^2 + 2|\nu|^2} < 2M. \quad (\text{D3b})$$

Furthermore, the moduli of the three eigenvalues of the matrix

$$\begin{pmatrix} \lambda_1 & -\sqrt{2}|\nu| & \sqrt{5/2}\lambda_4 \\ -\sqrt{2}|\nu| & \lambda_3 + (5/4)\lambda_4 & 0 \\ \sqrt{5/2}\lambda_4 & 0 & \lambda_2 - (11/5)\lambda_5 \end{pmatrix} \quad (\text{D4})$$

must all be smaller than M .

When $V_{4,\text{extra}} = 0$ the unitarity conditions for all three models are identical, *viz.* conditions (D1a)–(D1e), (D1f), (D1h), (D1i), and

$$|\lambda_3| + \frac{5}{4}|\lambda_4| < M. \quad (\text{D5})$$

They coincide with the unitarity conditions for the case $J = 3/2$ in Ref. [14].